DETECTION OF ATHEROSCLEROTIC CORONARY PLAQUES BY FLUORESCENCE LIFETIME IMAGING ANGIOSCOPY

A Thesis

by

PATRICK ALLEN THOMAS

Submitted to the Office of Graduate Studies of
Texas A&M University
in partial fulfillment of the requirements for the degree of

MASTER OF SCIENCE

August 2010

Major Subject: Biomedical Engineering

DETECTION OF ATHEROSCLEROTIC CORONARY PLAQUES BY FLUORESCENCE LIFETIME IMAGING ANGIOSCOPY

A Thesis

by

PATRICK ALLEN THOMAS

Submitted to the Office of Graduate Studies of
Texas A&M University
in partial fulfillment of the requirements for the degree of

MASTER OF SCIENCE

Approved by:

Chair of Committee,	Javier Jo
Committee Members,	Fred Clubb
	Kristen Maitland
Head of Department,	Gerard Cote

August 2010

Major Subject: Biomedical Engineering

ABSTRACT

Detection of Atherosclerotic Coronary Plaques by

Fluorescence Lifetime Imaging Angioscopy.

(August 2010)

Patrick Allen Thomas, B.S., Louisiana Tech University

Chair of Advisory Committee: Dr. Javier Jo

Vulnerable plaque is a clinically silent condition of atherosclerotic plaque that leaves a large number of patients at risk of a coronary event. A method to detect vulnerable atherosclerotic plaque would greatly enhance the ability of clinicians to diagnose and treat patients at risk. Fluorescence lifetime imaging microscopy (FLIM) offers a way to extract both spatial and biochemical information from plaque by taking several wide-field images over time. The goal of this study was to determine the potential of a FLIM angioscopy system to detect and differentiate coronary atherosclerotic plaques ex-vivo into several groups including thin, fibrotic, lipid-laden, thick-cap fibroatheroma (FA), and fibrocalcified.

Samples were extracted post-mortem weekly and sliced open to have their lumens imaged. For each sample, 51 time resolved wide-field images were taken over 10 nanoseconds at 390 (±40) nm, 450 (±40) nm, and 550 (±88) nm wavelengths. To analyze the samples, the intensity map and lifetime map were created at each wavelength. The intensity map was simply the wide-field images summed in time and normalized. In

order to calculate lifetime at each point, a fast, model-free Laguerre deconvolution algorithm was recently developed for FLIM data analysis and was used. This allowed for fast, efficient estimations of the fluorescence decay curves at each pixel of the FLIM images and facilitated the computation of quantitative parameters describing the fluorescence emission of the tissue, specifically, the relative fluorescence intensity and lifetime at defined emission bands.

Statistical analysis on these FLIM derived parameters indicated that the autofluorescence emission of the plaques allows for distinguishing relative plaque thickness: thin plaque, whose signal is dominated by elastin fluorophores, shows a marked difference between thicker plaques, such as fibrotic, fibrocalcified and thick-cap FA (who are dominated primarily by collagen). However, the ability of the current FLIM system to differentiate vulnerable plaque remains in question due to the absence of thin-cap FA samples. Further work has also been proposed; of primary concern is gathering thin-cap FA plaque samples needed to validate the system's ability to differentiate vulnerable plaques from other common groupings.

DEDICATION

For my parents, Greg and Terry, and my grandparents, both here and gone. I also dedicate this to Keri for all of her support and patience. Thanks for staying on board, no matter how long the road has been.

ACKNOWLEDGEMENTS

I would like to acknowledge my graduate advisor, Dr. Javier Jo, for the help and encouragement he has given throughout my academic and research career at Texas A&M. Without his support and guidance, I would not be where I am now. He has made my time here productive, meaningful and fulfilling. Thank you for supporting me, both financially and my work, and seeing this process through to the end.

My lab-mates who have given me feedback and assisted me also deserve to be recognized. They have been an immense help in explaining various programs, systems, and the math needed to bring my project to completion. I would be here much longer without them to help me.

To my friends and family, thank you for teaching me to keep going. This has been a key to many of the problems I have faced throughout my time here and in my undergraduate career. Without them, I wouldn't even have a chance to be where I am today.

TABLE OF CONTENTS

Page

ABSTRACT iii

DEDICATION v

ACKNOWLEDGEMENTS vi

TABLE OF CONTENTS vii

LIST OF FIGURES ix

LIST OF TABLES x

1. INTRODUCTION 1

2. BACKGROUND 3

    2.1 Atherosclerosis 3
    2.2 Current Intravascular Imaging Methods of Atherosclerosis 4
    2.3 Fluorescence Lifetime Imaging Microscopy (FLIM) 8
        2.3.1 Fluorescence 8
        2.3.2 Fluorescence Lifetime Imaging Microscopy 11

3. METHODS 14

    3.1 FLIM System and Sample Recording 14
    3.2 Histology 15
    3.3 Laguerre Deconvolution and the Acquisition of the True Response ... 16
        3.3.1 Lifetime Deconvolution Techniques 16
        3.3.2 Laguerre Deconvolution 17
    3.4 Processing and Data Analysis 19
        3.4.1 Initial Processing 19
        3.4.2 Determining Optimal α for All Datasets 20
        3.4.3 Measurement of the Instrument Response 21
        3.4.4 Photobleaching Testing 21
    3.5 Parameter Correlation to Histological Features 22

4. RESULTS 24

Page

4.1 Results of α Value Optimization 24
4.2 Histological Data 24
4.3 FLIM Data Analysis 28
4.3.1 Histological Grouping Analysis 28
4.3.2 Fibrotic Plaque Thickness Analysis 33

5. DISCUSSION AND CONCLUSIONS 36

5.1 Discussion 36
5.2 Future Scope 40
5.3 Conclusions 41

REFERENCES 42

APPENDIX 45

VITA 46

LIST OF FIGURES

FIGURE		Page
1	Jablonski Diagram	9
2	Thin Plaque Histology and Corresponding FLIM Image Recorded at 390nm, 450nm, and 550nm Wavelengths. The Elastin From the Lamina Dominates the Fluorescent Signal. This Is Indicated by Higher Intensity at 450nm, and Lower Lifetime Values.	26
3	Fibrotic Plaque Histology and Corresponding FLIM Image Recorded at 390nm, 450nm, and 550nm Wavelengths. The Collagen From the Plaque Dominates the Fluorescent Signal. This is Indicated by Higher Relative Intensities at Lower Wavelengths, Which Gradually Decrease, and Higher Lifetime Values.	27
4	Multicomparison Test Results of Significant Parameters When Analyzing by Histological Grouping	31
5	Intensity and Lifetime Comparison of Data Grouped by Plaque Thickness at 390 nm	35

LIST OF TABLES

TABLE Page

1 Mean and Standard Deviation of α Values, and P-value Comparison of Groups by Wavelength 24

2 ANOVA and T-test P-values at 390, 450, and 550 nm for FLIM Intensity, Lifetime, and First Two Laguerre Coefficients. The Histological Groupings Were Consolidated Into the Following Groups: a) Thin, b) Fibrotic and Thick Cap FA, and c) Fibrocalcified 29

1. INTRODUCTION

Fluorescence imaging has the potential to extract biochemical information from tissue (1-3). In some cases, utilizing the autofluorescent signal produced by biological fluorophores in the tissue of interest leads to distinguishing normal conditions from pathologically effected tissue (4-5). This is possible because every known fluorophore possesses unique excitation and emission spectra, allowing biochemical information to be determined. Sometimes, however, these spectra overlap significantly, posing a problem in discerning fluorophores, especially when two or more are present in the region of interest. Fortunately, a second parameter known as the fluorescence lifetime, which describes the time it takes for an emission to decay in intensity after stimulation, may be used as a way to identify fluorophores. Fluorescence lifetime imaging microscopy (FLIM) utilizes both spatially and temporally resolved information to distinguish fluorophores in space for size measurements as well as chemical identification.

This thesis follows the style of *Journal of Photochemistry and Photobiology*.

The purpose of this research was to examine the potential of FLIM to characterize biochemical composition of atherosclerotic coronary plaques. To fulfill this objective, the two specific aims of this work were:

- Aim 1: Collect a database of FLIM data images from post-mortem human coronary plaques and their underlying histopathology. A FLIM angioscope was used to image the lumen of coronary plaques. The imaged plaque tissue sections were sent for histopathology analysis. Plaques were procured and imaged from 15 subjects.
- Aim 2: Determine a set of FLIM features that could allow the quantification of plaque composition. The FLIM images were processed to derive a set of parameters quantifying the plaque autofluorescence (such as relative intensity and lifetime values at different emission bands). The resulting parameters were statistically correlated to the plaque histopathology.

In the following work, the FLIM system's ability to differentiate ex vivo coronary plaque types is investigated. It was found that intensity, lifetime, and laguerre expansion coefficients were good identifiers of certain plaque types, primarily based on plaque thickness due to shifts in dominant fluorophores. Elastin gives a strong fluorescent signal with thin plaques, while collagen dominates the fluorescent signal in thick plaques and calcified plaques. Unfortunately, very little plaques with thin cap fibibroatheromas were available, making it impossible to perform statistical analysis on vulnerable plaques.

2. BACKGROUND

2.1 Atherosclerosis

Atherosclerosis is an intravascular disease in which lipids build up in the lumen of a blood vessel over time. This condition can lead to several life-threatening complications. In 2008, 1.49 million Americans suffered from a myocardial infarction, in which 560,000 did not survive (6). About 70% of all coronary events are related to the rupture of atherosclerotic plaque buildup, primarily due to thrombosis at the plaque rupture site (7). Plaque buildup begins early in life as a simple aggregate of lipid cells entrenched in a collagen matrix on the surface of the lumen. As the plaque becomes larger, inflammatory cells migrate into the site and begin to metabolize the lipid cells, forming foam cells. As time goes on, a collagen matrix begins to wall off the lipid core. The cap, or the collagen-lipid matrix between the lumen and the core, may be thick enough to withstand shear forces from the blood flow, leading to a stable plaque. On the other hand, thin cap plaques (usually having < 65μm cap thicknesses) are prone to rupture and referred to as thin-cap fibroatheromas (TCFA) (8). Vulnerable plaque is specifically defined as mildly to moderately stenotic plaque that are precursors to coronary thrombosis and myocardial ischemia (9). TCFA is one of the major types of vulnerable plaque, causing a thrombolytic response at the rupture site, subsequently leading to partial or complete occlusion of the vessel. This study focused primarily on differentiating TCFA and the lipid core below it to analyze vessel plaques.

Patients prone to atherosclerotic buildup include age, lipid-rich diet, and genetics. Lipids buildup often goes unnoticed until a coronary event occurs, thus making atherosclerosis clinically silent. Without a simple, definitive method to determine plaque vulnerability, atherosclerosis will continue to be a prevalent cause of coronary events, and therefore fatal incidents, around the world.

2.2 Current Intravascular Imaging Methods of Atherosclerosis

The first and most established technique for intravascular detection of atherosclerotic plaque is Intravascular Ultrasound, or IVUS. IVUS is the adaption of ultrasonography to intravascular applications and returns A-line scans (A-line scans are lines of spatially resolved information which radiates from the detector at some certain angle). These A-line scans are taken as the IVUS catheter rotates, producing cross sectional images called B-scans. However, this technique suffers from poor spatial resolution and the inability to differentiate soft tissue components (10). Furthermore, calcium deposits, which are common sites of late-stage atherosclerotic plaque, are easily identifiable due to the radial “shadows” they leave behind them due to their ability to largely absorb acoustic waves. This presents a problem by masking any features behind the calcium deposit (11).

Optical Coherence Tomography (OCT) presents another way to scan the physical tomography of a surface, giving similar information as IVUS. OCT has received a decent amount of attention in recent years for its high spatial resolution. Some groups have found that it can detect macrophages, a sign of plaque vulnerability (12-13). OCT

has not yet become a mainstream technique for intravascular plaque detection, however. OCT utilizes optical interferometry to reconstruct spatial images of the vessel wall by comparing the phase and intensity differences between the reference optical path and the optical path that interacts with the vessel (10). This method scans the surface to construct diagnostically relevant images, eventually producing cross sectional images of the blood vessel of interest through A-line scanning. The axial resolutions of current OCT systems are between 10 and 20μm, although highly scattering mediums such as hemoglobin may increase these numbers (10, 14-15). OCT is advantageous for detecting TCFA's because of its ability to gather microscopic information from the surface of plaques (9) and its high resolution. However, 3D scanning requires saline flushing of the vessel to offset the effect of hemoglobin and water absorption and reduce noise. Finally, OCT generates purely structural and morphological information, with little to no biochemical information accessible. Thus, it would be advantageous if OCT were coupled with other optical methods to gain a full view of the nature of the plaque.

Optical Spectroscopy techniques, including Fluorescence, Raman and NIR Spectroscopies, have also been explored as methods to detect plaques. Fluorescence is a specific response to photon excitation that results in the unique emission of photons at wavelengths longer that the excitation wavelength. The unique emission of various fluorophores allows for chemical composition detection of the illuminated area. It is possible to recover spatially resolved images with fluorescence, depending on collection mechanism. The excitation wavelength tends to be either in the UV range or visible range to maximize excitation of the fluorophores intrinsic in the tissue (16-18).

Fluorescence spectroscopy receives its contrast by varying degrees of fluorescent intensity response as a function of emission wavelength. Fluorescence spectroscopy alone, without being temporally resolved, usually involves ratiometric measurement of a single point at different wavelengths, and has detected plaque ex vivo (18). A major advantage of this method is that it is a proficient detector of atherosclerotic plaque, and the ease of recording a sample's entire spectral response to excitation. However, it lacks sufficient spatial information to gauge intravascular plaque sizes. Temporally resolved measurements, as seen in Fluorescence Lifetime Imaging Micrcosopy systems, are more robust due to relative intensity measurement required for fluorescence lifetime calculation, as well as an added lifetime parameter to characterize plaques.

Raman spectroscopy is a non-destructive optical technique that acquires biochemical information of the tissue and can specifically target calcium-laden and cholesterol-laden plaques (19). Raman spectroscopy excites in the NIR and IR wavelength range to observe changes in excitation of vibrational energy states, rather than the larger electronic states of atoms and molecules. Raman has been combined with other modalities, such as Diffuse Reflectance Spectroscopy (DRS) or Fluorescence Spectroscopy (20). A major advantage to this technique is that these vibrational energy peaks are very specific to bonding types and atoms in a molecule, thus making it easier to identify bulk biological compounds. The disadvantages of this technique are threefold: first, the low signal level resulting in a long signal integration time (the amount of time the recording element collects a signal in a given recording period) required. Some report collection times of up to 100 seconds (21), which becomes a

problem when taking measurements in a clinical setting: longer recording times increase the probability of artifacts and risk to the patient. Second, fluorescence emission usually is present when recording Raman signals, and must somehow be separated from the intended Raman signal. Third, this technique cannot extract a significant amount of depth information past a few hundred micrometers (19). Although Raman spectroscopy affords a great deal of biochemical information, the ability to spatially resolve the region of interest would be invaluable in evaluating the size and thickness of necrotic cores and other signs of vulnerable plaque.

Intravascular NIR Spectroscopy is advantageous because blood absorption does not occur as prominently at these wavelengths. NIR Spectroscopy measures both absorption and scattering spectra to characterize cholesterol and collagen content in plaques (22). NIR and Mid-IR detection systems also penetrate deeper into tissue, a definite advantage when differentiating vulnerable and stable plaques (23). However, NIR spectroscopy alone has difficulty correlating plaque thickness and lipid core depth, an important parameter of vulnerable plaque detection (24).

In summary, these techniques (OCT, IVUS, and Optical Spectroscopy techniques) have strengths and weaknesses, and none have yet been determined to be the definitive intravascular diagnostic tool for intravascular atherosclerotic plaque detection. Therefore, there is still room for investigating other techniques in atherosclerotic plaque differentiation.

2.3 Fluorescence Lifetime Imaging Microscopy (FLIM)

2.3.1 Fluorescence

When molecules and atoms absorb light, their electrons can transition from a ground state to an excited state. To return to ground state, the molecules may give off the absorbed energy as either radiative decay or non-radiative decay. If the electrons are in the more common singlet state, the electrons will emit energy quickly (within a few nanoseconds) as the electrons return to ground state (25). The energy released radiates at certain wavelength spectra, which equates to specific energy emission bands characteristic of the materials under illumination. The phenomenon of singlet-state energy radiative decay is known as fluorescence. Fluorophores, or materials that efficiently release energy in this manner (radiative decay), have been used for a variety of purposes, ranging from flow velocimetry to embryological development tracking (26-27). These uses are made possible due to several hundred different fluorophores having unique absorption and emission spectra, as well as unique lifetime. The absorption spectrum represents the efficiency of photon absorption across varying wavelengths. Similarly, the emission spectrum describes the efficiency of the excited fluorophore to emit photons at varying wavelengths. The lifetime describes a fluorophore's tendency to emit photons as a function of time.

These two spectra differ due to a phenomenon known as the Stoke's Shift, which is a result of photons emitted having less energy than the photons used to excite the fluorophore. Specifically, the wavelength of an incoming photon to be absorbed by the fluorophore can be represented by some amount of energy through Planck's Law:

$$E = h\frac{v}{\lambda} \quad (1)$$

E is the energy of a single photon, h is Planck's constant, v is the velocity of the photon (a function of the medium it is traveling through), and λ represents the wavelength, usually in nanometers. All materials have quantifiable energy levels that determine the energy required to excite an electron from its ground state to an excited state, making fluorescence possible.

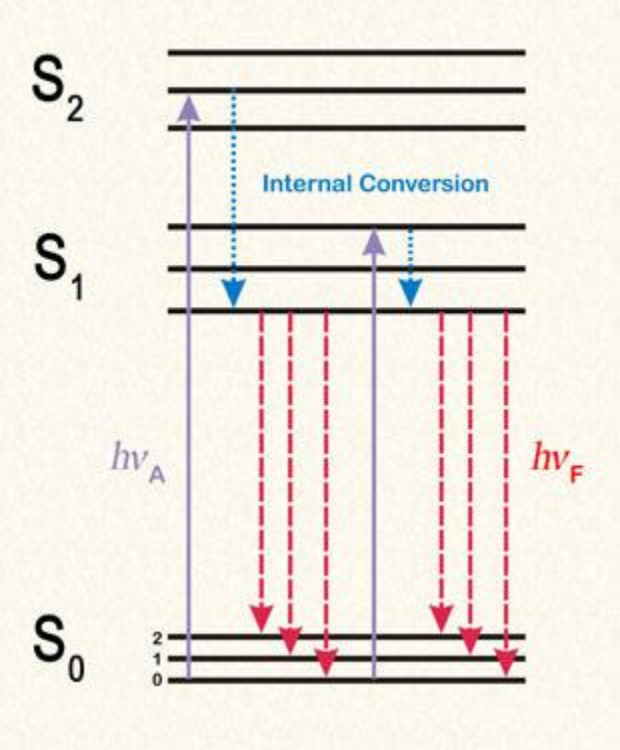

Figure 1. Jablonski Diagram (28).

The Stoke's Shift will be explained with the help the Jablonski Diagram (Figure 1). As energy in the form of photons enter the system, electrons leave their resting

electronic state (S_0) to occupy a higher electronic state, denoted by S_1 and S_2. An electron may occupy any vibrational energy state upon excitation, shown in Figure 1 as the lines within each electronic state with small increments between each other. Excited molecules lose some energy in the process known as internal conversion prior to returning to ground state, as illustrated. After internal conversion, the electrons of a fluorophore will then release the rest of its absorbed energy by emittiong a photon, forming the fluorophore's emission discussed earlier. Not all electrons will emit a photon to return to ground state: the quantum yield is a measure of the amount of photons emitted vs. the number of photons absorbed. The intensity spectrum absorbed is primarily a function of the quantum yield, excitation wavelength, and molar extinction coefficient (the absorbing power) of the fluorophore of interest (25).

With a sample of a single fluorophore type, the fluorescence intensity will generally follow a single exponential decay as more and more individual fluorophores emit photons, returning to ground state. Fluorescence lifetime follows first order kinetics and can be calculated using the following equation:

$$F(t) = \sum_{i=0}^{n} F_o e^{-t/\tau_n} \quad (2)$$

The lifetime τ_n is related to the decay rate of the excited species, and is given by equation 3:

$$\tau_n = (\Gamma + k_{nr})^{-1} \quad (3)$$

Lifetime changes across the emission spectrum in complex fluorescence systems such as tissue, making it a powerful parameter to further identify fluorophores that may have similar or overlapping emission spectra. In the case of such systems, multiple

fluorophores usually are present and can be represented by a multiexponential summation of n fluorophores. In this research, three fluorophores intrinsic to blood vessels and plaque are stimulated: collagen, elastin, and lipids. These three fluorophores allow for marker-less fluorescence measurements and the possibility of plaque detection via fluorescence and lifetime measurements.

The issue of penetration depth should be discussed in brief. There is a limit to how deep a fluorophore may be imaged due to adsorption and scattering in the sample medium as well as the limitations of optical setup. In the case of vulnerable atherosclerotic plaque detection, a penetration depth of 65μm (the thickness of a thin cap FA) or higher is required to differentiate thin cap FA's. Higher penetration depths are desired, however, in order to extract more information about the biochemistry of the underlying core. With an UV excitation (~337 nm) into vessel tissue, the penetration depth is expected to be roughly 200 μm, which should adequately extract fluorescent signals from lipid cores with thin caps (1).

2.3.2 Fluorescence Lifetime Imaging Microscopy

Fluorescence Lifetime Imaging Microscopy (FLIM) is an imaging modality that spatially resolves fluorescence lifetime information from a sample, which in turn provides biochemical information in the field of view. Wide-field time-gated imaging, the specific FLIM modality utilized in this study, gathers a series of temporally wide field images to build intensity and lifetime profiles in the field of view. There are several potential advantages of using FLIM for VP detection. First, FLIM spatially resolves

fluorophores over the field of interest, making it possible to identify the size of plaque features. Secondly, by using relative intensity measurements, lifetime parameters can be extracted even at low signal strength: light absorbers and the optical path of the system will not alter lifetime measurements. This also allows the intensity measurements between samples to be different while still allowing meaningful comparison of lifetimes between samples. Finally, the extra parameter of lifetime gives additional ways to analyze fluorescence data for biochemical, and thus histopathological, characterization. These equate to a robust measurement modality that may have potential for atherosclerotic plaque detection.

Provided that the field of view is large enough, FLIM can potentially determine plaque features like collagen-rich plaques and necrotic cores, due to changes in fluorescence intensity and lifetime throughout the sample. When coupled with other modalities, FLIM can reinforce the findings of other imaging modalities looking at morphological structure (29). In the mentioned paper, OCT and FLIM are utilized in tandem to extract both morphological and biochemical information of the region of interest. The fluorophores of interest lend themselves to fluorescence lifetime techniques due to their overlapping intensity emission spectra. Collagen has a higher intensity measurements than elastin at 390 nm, and elastin peaks at roughly 450 nm; however, a large amount of overlap remains. Lifetime measurements show very distinct lifetimes at lower wavelengths (elastin: ~2 ns, collagen: 1-1.5 ns), making FLIM an ideal choice for spatially mapping collagen, and therefore plaque, in coronary vessels (30-31). The added

lifetime parameter therefore places diagnostically relevant features into more differentiable categories by increasing the amount of fluorescence information available.

Finally, Fluorescence Lifetime Imaging Microscopy offers a relatively high signal-to-noise ratio. This avoids overly-high integration time, as seen frequently in Raman Spectroscopy, making signal collection faster and more reliable in a heterogeneous environment. FLIM therefore deserves to be explored as a detection modality for vulnerable atherosclerotic plaques.

3. METHODS

3.1 FLIM System and Sample Recording

The FLIM setup is a wide-field time-gated system with a field of view of 3mm (diameter). The FLIM angioscope is bifurcated, consisting of a common distal end containing 10,000 bundled, coherent collection fibers (350/450 μm inner/outer diameter, Fujikura, Japan) surrounded by 200 illumination fibers (50/66 μm inner/outer diameter, 0.22 NA, High OH silica/silica for UV transmission). The distal end of the imaging probe was cemented to a gradient index objective lens (350 μm diameter, 0.5 NA, 4 mm working distance, GRINTECH GmbH, Germany). The distal end splits into two proximal ends: the proximal illumination fiber and the proximal collection fiber. The proximal illumination fiber terminates with a SMA-905 connector, and the proximal collection bundle was flat polished. The entire fiber bundle is ~2m long and has an outer diameter of 2mm at the distal (thicker) end.

A digital signal delay generator synchronizes the ICCD camera gating with the pulsed laser illumination. The pulsed nitrogen laser (Center wavelength~337nm, 700 ps pulse width, MNL 205, LTB Lasertechnik, Germany) sends a pulse at 50 Hz, entering the proximal illumination fiber bundle, and reaches the XYZ sample stage containing the artery sample. The sample generates a fluorescent signal, illuminates the collection bundle, coherently travels through the collection bundle, and exits into a short optical train, beginning with a 20x microscope lens followed by a 15cm focal length doublet lens, which forms an infinitely corrected microscope configuration. Before reaching the

doublet lens, the magnified signal travels through a mechanical lens filter with three bandpass wavelengths: 390±40nm, 450±40nm, and 550±88nm. These wavelengths have been determined to be optimal for differentiating fluorophores intrinsic to atherosclerotic plaques (17). The gated intensified charge-couple device (ICCD) camera (4Picos, Stanford Computer Optics, Berkeley, CA) records the remaining passed signal at various delays in 200 ps intervals, such that wide field images at different delays compile to form both a spatially and temporally resolved image. The spatial resolution of the resulting images is ~50µm, and the temporal resolution is approximately 0.5ns. The penetration depth of the system has been calculated to be roughly 200µm, which is sufficient to identify thin cap FA's.

The ICCD camera recorded 51 images, each separated by 200ps in time (for a total recording time of 10ns). The open gate time per image was 200ps. Each image was comprised of 25 frames to ensure a brighter and more stable intensity map for analysis. Each recording took approximately 60 seconds due to slow repetition rate of the laser, the long integration time and high amount of frames in each recording experiment.

3.2 Histology

The coronary samples were imaged within 48 hours of receiving the tissue, keeping the vessels wet with Phosphorous buffer solution (10% diluted in DI water). After imaging, the pieces were processed following standard histopathology protocols and stained with Movat pentachrome. Movat staining is a common cardiovascular stain useful in differentiating collagen, elastin, smooth muscle cells, macrophages and

necrotic cores (29). Collagen is stained blue, while the external and internal elastic laminas show up as red with the surrounding area showing up as dense black lines (due to elastin). Foam cells are hollow (due being dissolved by alcohols in the preservation and staining process) with centrally red-stained nuclei. Lipid cores are mostly hollow with centrally red-stained nuclei. ms study aimed to evaluate the ability of FLIM to differentiate between thick cap fibroatheroma (cap >65μm) and thin cap fibroatheroma (cap <65μm). The groups used in this study include thin fibrotic plaque (<100μm), thick fibrotic plaque (>100μm), fibrocalcified plaque, thin-cap fibroatheroma, and thick-cap fibroatheroma.

3.3 Laguerre Deconvolution and the Acquisition of the True Response

3.3.1 Lifetime Deconvolution Techniques

The camera records fluorescent signals that are convolutions of the impulse response of the fluorophore and the laser profile. Thus, to determine the proper lifetime of any region of the FLIM image, the fluorescence decay at each pixel of the image must be deconvolved. The most common methods to accomplish this include non-linear least-square iterative reconvolution (32-33) and rapid lifetime determination (RLD) (34). The non-linear least-square iterative method can be a powerful technique because it does not assume an input profile of negligible width. This method uses a least-squares optimization algorithm to fit the data to a multiexponential decay model to deconvolve the impulse response from the input. However, this method suffers from long calculation times, making it a poor choice for the purpose of wide-field FLIM analysis. In contrast,

Rapid Lifetime Determination can deconvolve large amounts of data quickly. RLD relies on the fact that the input profile is of negligible size, an unfair assumption of the FLIM apparatus used in this study. Laguerre deconvolution, the method used in this study, offers both accuracy and speed in deconvolving spatially resolved FLIM data. This method has recently been introduced and validated as a method for deconvolving FLIM images (35-36). Laguerre deconvolution owes its speed to the fact that the impulse response at each pixel is a summation of weighted Laguerre functions, effectively forming a basis for the entire image. This can be performed across the entire image simultaneously, up to two orders of magnitude faster than previously discussed algorithms (35).

3.3.2 Laguerre Deconvolution

The following equations outline the mathematics behind Laguerre deconvolution. The recorded intensity profile reflects the instrument response, or input, convolved with the fluorescence emission:

$$H(\mathrm{r_x}, \mathrm{r_y}, \mathrm{n}) = T \sum_{m=0}^{K-1} h(\mathrm{r_x}, \mathrm{r_y}, \mathrm{m}) x(n-m) \quad n = 0, \dots, K-1 \qquad (4)$$

The equation above illustrates the decay function $H(r_x, r_y, n)$ in discrete time, a convolution of the impulse response function (IRF) $h(r_x, r_y, n)$ and the instrument response x(n). In this study, we will apply the Laguerre deconvolution method to recover the IRF at each pixel of the image, chosen for both its efficiency and accuracy in deconvolving images in 2D (35). In this method, the IRF is modeled as a linear expansion on a set of orthonormal Laguerre functions:

$$h(r_x, r_y, n) = \sum_{j=0}^{L-1} c_j(r_x, r_y) b_j^{\alpha}(n) \quad (5)$$

Here, $c_j(r_x, r_y)$ denotes the Laguerre expansion coefficient (LEC) computed at each pixel, and the Lageurre basis function b(n) is defined as follows:

$$b_j^{\alpha}(n) = \alpha^{(n-j)/2}(1-\alpha)^{1/2} \sum_{k=0}^{j}(-1)^k \binom{n}{k} \times \binom{j}{k} \alpha^{j-k}(1-\alpha)^k \quad (6)$$

α denotes the efficiency of b(n) to match the fluorescence decay by changing the rate at which the Discrete Laguerre Function decays. For any value of α, j orders can be used to estimate the decay function. Conversely, a set amount of orders can be used to optimize α for each data set. With equations 4-6, we can write an equation that describes the recorded image pixel by pixel using Laguerre expansions:

$$y(\mathrm{r_x}, \mathrm{r_y}, \mathrm{n}) = \mathrm{H}(\mathrm{r_x}, \mathrm{r_y}, \mathrm{n}) = \sum_{j=0}^{L-1} c_j(r_x, r_y) v_j^{\alpha}(n) \quad (7)$$

Where:

$$v_j^{\alpha}(n) = T \sum_{m=0}^{K-1} h(\mathrm{r_x}, \mathrm{r_y}, \mathrm{m}) x(n-m) \quad (8)$$

Equation 6 can be written in matrix form in the following equation:

$$y_{\mathrm{r_x,r_y,n}} = \mathbf{V_{\alpha}} \mathrm{c}_{\mathrm{r_x,r_y,n}} \quad (9)$$

Where:

$$\begin{bmatrix} y(r,0) \\ y(r,1) \\ \vdots \\ y(r,N-1) \end{bmatrix} = \begin{bmatrix} v_0^{\alpha}(0) & v_1^{\alpha}(0) & \cdots & v_{L-1}^{\alpha}(0) \\ v_0^{\alpha}(1) & v_1^{\alpha}(1) & \cdots & v_{L-1}^{\alpha}(1) \\ \vdots & \vdots & \ddots & \vdots \\ v_0^{\alpha}(N-1) & v_1^{\alpha}(N-1) & \cdots & v_{L-1}^{\alpha}(N-1) \end{bmatrix} \begin{bmatrix} c_0(r) \\ c_1(r) \\ \vdots \\ c_{L-1}(r) \end{bmatrix} \quad (10)$$

An error term ε at pixel $(\mathrm{r_x}, \mathrm{r_y})$ was added to equation 9 to account for errors in measurement:

$$y_{\mathrm{r_x,r_y,n}} = \mathbf{V_{\alpha}} \mathrm{c}_{\mathrm{r_x,r_y,n}} + \varepsilon_{\mathrm{r_x,r_y}} \quad (11)$$

Previous work has found that L=4 orders of the Laguerre equations sufficiently reproduces the deconvolved decay curve (37). The final output of the deconvolution is then the Laguerre expansion coefficients $c_{rx,ry,n}$ and α, which provides the information needed to construct the true decay of the signal.

3.4 Processing and Data Analysis

3.4.1 Initial Processing

Immediately following recording of the FLIM dataset, the data was spatially decimated by using a moving average across the entire image set. Temporal resolution was preserved in order to maximize accuracy of deconvolution and lifetime measurements, while still decreasing the file size to something more manageable. This also has the added benefit of smoothing out noise in the signal due to fluctuations in the recorded intensities (improving the signal to noise ratio).

The following discusses how the algorithm determines the optimal value for α in a given sample. In order to obtain a proper impulse response function (IRF), the correct value for α ($0<\alpha<1$) must be determined. After decimating the image, an instrument response delay was selected, followed by optimizing the α parameter of the sample. In the following equation, $\hat{y}$ is the least-square solution for the measured decay function, and is an estimation of the decay function using the Laguerre vectors defined in equations 9 and 10:

$$\hat{y}(\mathrm{r_x}, \mathrm{r_y}, \mathrm{n}) = \boldsymbol{V_\alpha}\left(\boldsymbol{V_\alpha}^T \boldsymbol{V_\alpha}\right)^{-1} \boldsymbol{V_\alpha}^T y(\mathrm{r_x}, \mathrm{r_y}, \mathrm{n}) \quad (12)$$

The error of fit between the least-square estimation and the recorded signal ε_r can be defined as:

$$\varepsilon_{r_x,r_y} = y_{r_x,r_y} - \hat{y}_{r_x,r_y} \quad (13)$$

Therefore, a cost function $P_{r_x,r_y}(\alpha)$ at a given pixel (r_x,r_y), or a scalar value that defines the quality of fit between the measured signal and fitted signal is defined as:

$$P_{r_x,r_y}(\alpha) = \left(y_{r_x,r_y} - \hat{y}_{r_x,r_y}\right)^T \left(y_{r_x,r_y} - \hat{y}_{r_x,r_y}\right) = {y_{r_x,r_y}}^T \varepsilon_{r_x,r_y} \quad (14)$$

The cost of an entire image is given as the summation of the entire image. The optimum value for α yields the lowest image cost function. The optimization algorithm uses the cost function of equation 14 by first selecting a value for α, starting with α=0.5. The cost function's derivative is then calculated: the optimal value of α will yield a slope of 0.

Once the algorithm finds an optimal α solution, it stores its cost, and compares it to the cost of other optimal α values calculated with different instrument response delays. Finally, the algorithm selects an optimal delay and α associated with the lowest cost function, and performs Laguerre deconvolution. A more detailed explanation to optimizing α in the case of time-resolved fluorescence spectroscopy has been published in (37).

3.4.2 Determining Optimal α for all Datasets

In order to decrease processing time and allow easier correlation between samples, we determined a single α value that could be used for analyzing the FLIM data from all samples. A previous set of 83 coronary arteries had their optimal value of α and

histological classification determined (38). Every sample initially optimized their α values separately. Each sample was imaged at 390nm, 450nm, and 550nm; therefore, each sample had three α values. To determine if a single value for α was appropriate, α values were grouped into categories by their wavelength. Student's two-tailed t-tests were performed between groups to determine if they were statistically similar. A p-value of $p>0.05$ was used to determine statistical significance for all t-tests performed. If statistically similar in all cases (390 nm vs. 450 nm, 390 nm vs. 550 nm, 450 nm vs. 550 nm), an average of all α values at all wavelengths would be averaged to produce a single α value to be used in future deconvolutions.

3.4.3 Measurement of the Instrument Response

The instrument response was measured by measuring the laser reflection on a mirror, which propagated into the collection bundle to be recorded by the ICCD camera. The recorded Full-Width Half-Maximum of the instrument response was determined to be ~ 1 ns, and is displayed in the Appendix (Figure A-1).

3.4.4 Photobleaching Testing

A series of images at peak fluorescence intensity was taken over several minutes to explore the effects of photobleaching on the sample. The sample was illuminated for 10 minutes, and an image was taken every minute (200 ns open gate time), starting at t=0 minutes for a total of 11 images. A sample of the data has been included in the Appendix (Figure A-2). The tissue suffered a 5% loss in fluorescence intensity at 10

minutes. Samples that will be used for statistical analysis take approximately 1 minute to record, making photobleaching negligible in our case.

3.5 Parameter Correlation to Histological Features

To produce the intensity map used in analysis, the intensities at each pixel were summed together into a single image. This became the overall intensity used in the analysis. Each sample was normalized by their respective maximum values after the sum of the time-resolved images was taken. The lifetime maps are lifetime values extracted from the impulse response functions at each pixel. The method of determining the impulse response function is outlined in section 3.3.2. Once the intensity maps of all samples were processed and deconvolved, the center region of the FLIM image, roughly one square millimeter, was selected for analysis. The average of the intensity, lifetime, and laguerre coefficients corresponding to the ROI were saved for statistical analysis. Each region was also assigned a histological classification based on the histological section correlating to the region: thin plaque, thick plaque, thin cap fibroatheroma, thick cap fibroatheroma, and fibrocalcified.

To determine if statistical significance existed between FLIM parameters and histological diagnosis, this study used multivariate one-paired ANOVA and student's two-tailed t-testing. The multivariate ANOVA test took into account all histological classifications and determined statistical significance if a group's average and spread differed from others. The student's t-test determines significant differences between two

selected classifications. P-values of 0.05 or less were viewed as statistically significant for both ANOVA and student's t-test.

The FLIM samples were also categorized into several groups by plaque thickness to investigate the potential of FLIM to measure plaque depth. In order to reduce histological variation, plaques classified as fibrocalcified, thin-cap and thick-cap were not included in this analysis. Each sample's central plaque thickness was recorded by measuring the sectioned sample with a microscope. These thickness measurements were made in the center to correspond to the center of the ROI selected on the FLIM image during analysis (the central 1x1 mm region). Samples were then broken into the following groups: plaque <0.05 mm, 0.05 mm < plaque < 0.10 mm, 0.10 mm < plaque < 0.20 mm, and plaque > 0.20 mm. Because elastin and collagen fluorescent signals are unique at 390 nm, 550 nm was not considered (17).

4. RESULTS

4.1. Results of α Value Optimization

As discussed in section 3.4.2, a single value for the α parameter would be advantageous in decreasing computation time while preserving accuracy of the Laguerre deconvolution. If the values of α are statistically similar regardless of emission band or histology grouping, a single, average value of α can be used for all samples. Table 1 summarizes the results:

Table 1. Mean and standard deviation of α values, and p-value comparison of groups by wavelength.

Wavelength	**Mean ± SE**	**Comparison**	**p-value**
390 nm	0.8096 ± 0.0004	**390nm vs. 450nm**	0.8872
450 nm	0.8102 ± 0.0003	**390nm vs. 550nm**	0.1756
550 nm	0.8157 ± 0.0003	**450nm vs. 550nm**	0.1250

Because all groupings were similar and had a p value of $p > 0.05$, an average value of $\alpha=0.8118$ was determined to be a sufficient approximation for all samples.

4.2 Histological Data

The data was classified into 9 groupings: 20 thin plaques, 60 fibrotic plaques, 1 thin cap FA, 12 thick cap FA, 17 fibrocalcified (a total of 110). Two samples representing coronary plaque can be seen in figure 2 and figure 3, as well as their

corresponding FLIM images. In the histological stains, both thin and fibrotic samples are given, respectively, which is reflected by the FLIM images by their differences in relative intensity and lifetime. The movat pentachrome stain causes the collagen to be light blue, whereas the internal and external elastic laminas contain dense, dark lines due to the elastin. Lipids are clear and were dissolved and removed due to the alcohols used in tissue preparation prior to sectioning and staining- few lipids are seen in the figures below. Foam cells, or lipid-filled inflammatory and smooth muscle cells, manifest themselves as clear spaces with red stained dots, representing the nucleus of the cell.

The FLIM images in figure 2 show that elastin is the dominant fluorophore in the vessel. Although there is some collagen present in the thin layer of plaque, and this signal did affect the overall recorded emission, the underlying elastin of the external elastic lamina contributed to the majority of the signal, as seen by a spike in intensity at 450nm, and smaller lifetimes across the recorded emission wavelengths. Figure 3, on the other hand, is dominated by the collagen found in the fibrotic plaque. The relative intensities of the corresponding FLIM images decrease with increasing wavelength, and the fluorescence lifetimes are higher than in thin plaque, which is expected (38).

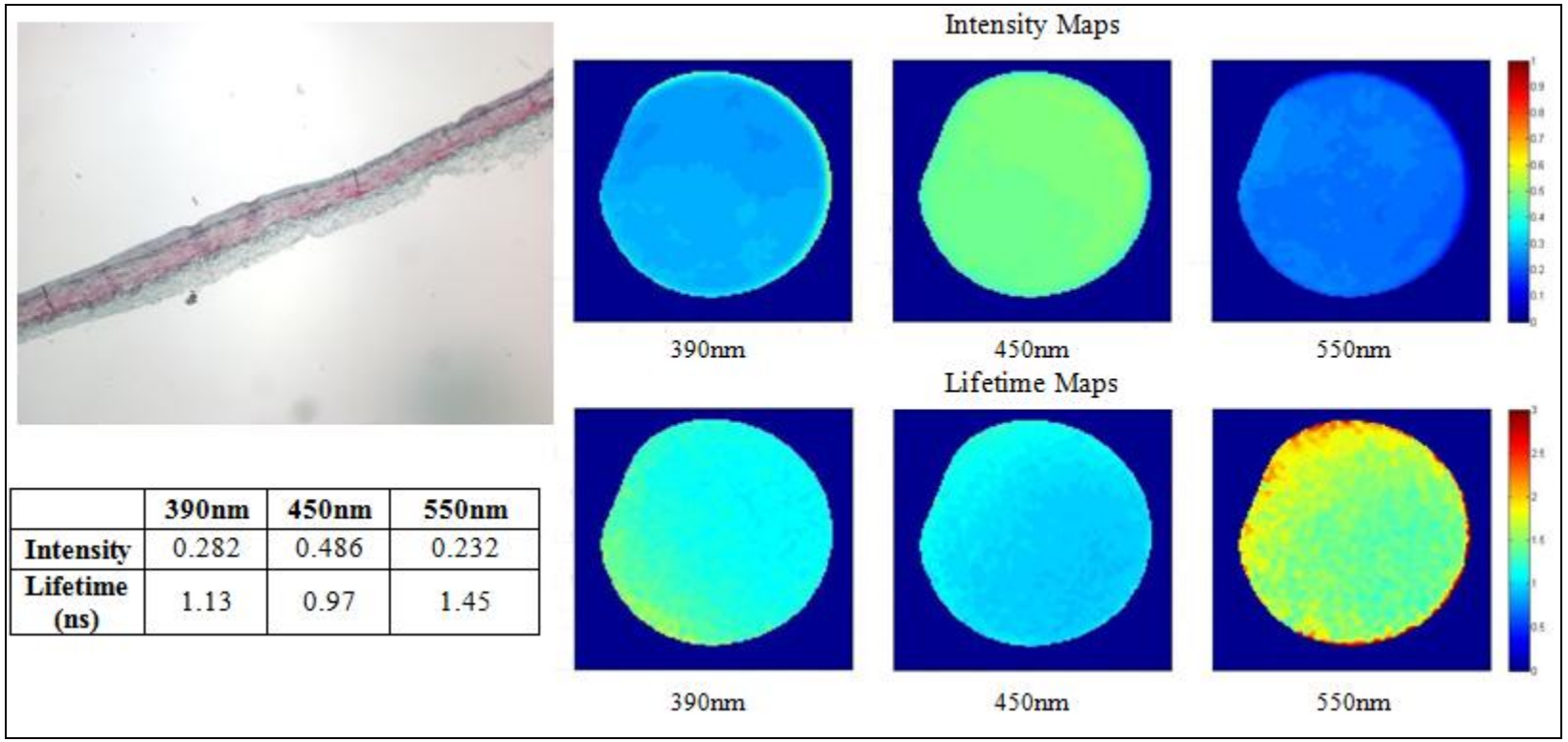

	390nm	450nm	550nm
Intensity	0.282	0.486	0.232
Lifetime (ns)	1.13	0.97	1.45

Figure 2. Thin plaque histology and corresponding FLIM image recorded at 390nm, 450nm, and 550nm wavelengths. The elastin from the lamina dominates the fluorescent signal. This is indicated by a higher intensity at 450nm, and lower lifetime values.

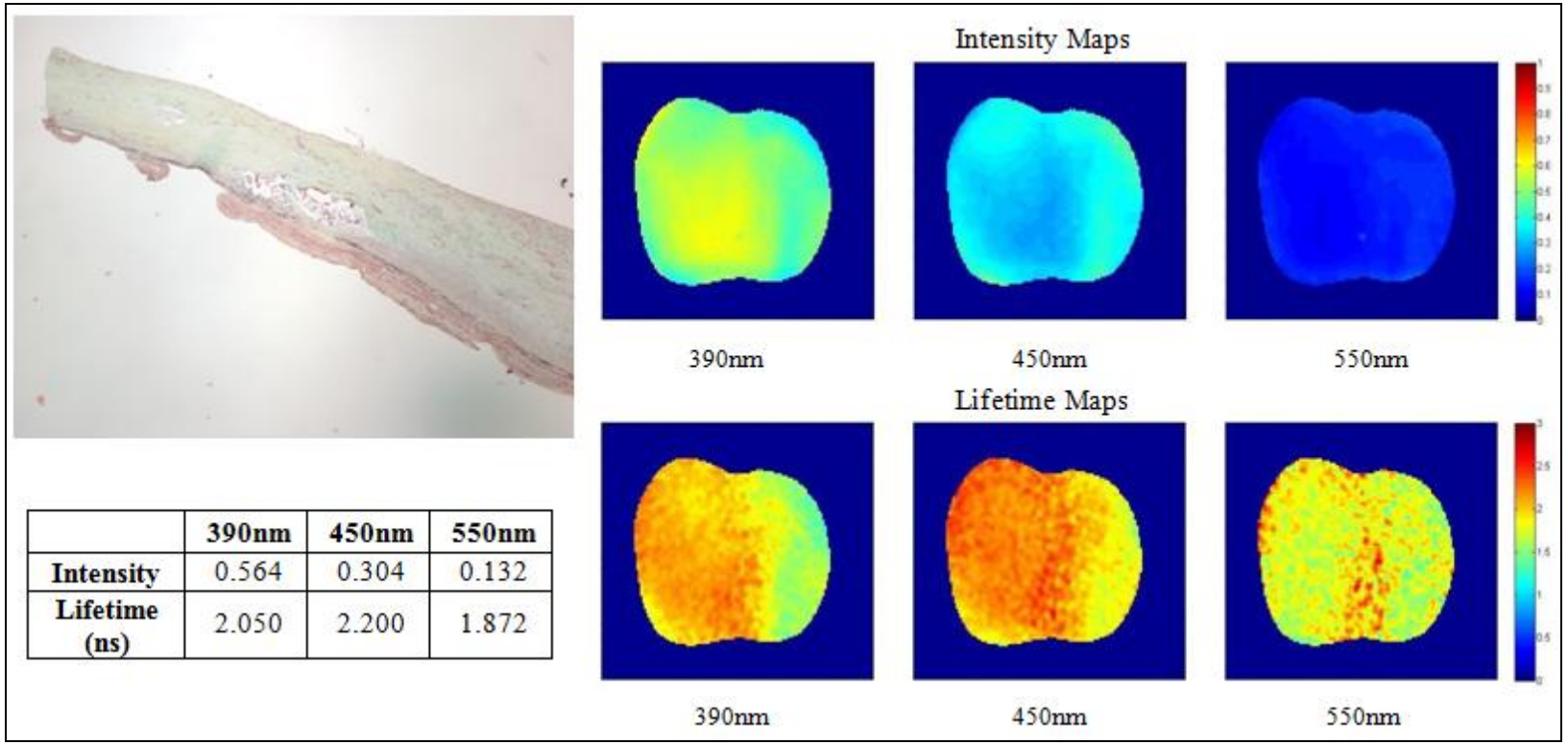

	390nm	450nm	550nm
Intensity	0.564	0.304	0.132
Lifetime (ns)	2.050	2.200	1.872

Figure 3. Fibrotic plaque histology and corresponding FLIM image recorded at 390nm, 450nm, and 550nm wavelengths. The collagen from the plaque dominates the fluorescent signal. This is indicated by higher relative intensities at lower wavelengths, which gradually decrease, and higher lifetime values.

4.3 FLIM Data Analysis

4.3.1 Histological Grouping Analysis

There was one thin-cap fibroatheroma in all samples recorded. There were 12 thick-cap FA's present. The following results focus on differentiating thin plaques, fibrotic plaques, and fibrocalcified plaques. When thick cap FA and fibrotic plaque samples were separated, their means and standard deviations overlapped significantly on both lifetime and intensity for all wavelengths, making them similar by the FLIM parameters used in this study. Therefore, fibrotic plaque samples were consolidated with thick-cap FA samples due to similarities in their signal. Table 2 shows the p-values associated with the ANOVA testing of the FLIM image's histological groupings remaining after consolidating inflamed groups to their non-inflamed counterparts, fibrotic and thick-cap FA, and removing thin-cap FA.

Table 2. ANOVA and t-test p-values at 390, 450, and 550 nm for FLIM Intensity, Lifetime, and first two Laguerre coefficients. The histological groupings were consolidated into the following groups: a) Thin, b) Fibrotic and Thick Cap FA, and c) Fibrocalcified.

FLIM Parameter	Band (nm)	Thin	Fibrotic	Fibro-Calcified	ANOVA p-value	Thin v. Fibrotic p-value	Thin v. Fibro-Calcified p-value	Fibrotic v. Fibro-Calcified p-value
Normalized Intensity	390	0.3410 + 0.0196	0.3972 + 0.0103	0.3935 + 0.0213	**0.0410**	**0.0007**	0.0719	0.8950
	450	0.4604 + 0.0123	0.4143 + 0.0065	0.4057 + 0.0133	**0.0024**	**0.0002**	**0.0093**	0.6432
	550	0.1987 + 0.0099	0.1885 + 0.0052	0.2008 + 0.0108	0.4640	-	-	-
Lifetime (ns)	390	1.1542 + 0.0827	1.5620 + 0.0436	1.4537 + 0.0897	**0.0002**	**3.75E-06**	**0.0085**	0.2814
	450	1.4057 + 0.0812	1.4872 + 0.0428	1.5854 + 0.0880	0.3282	-	-	-
	550	1.3718 + 0.0785	1.6210 + 0.0414	1.5692 + 0.0851	**0.0223**	**0.0005**	0.0748	0.6186
LEC 1	390	0.7552 + 0.0164	0.8305 + 0.0087	0.8232 + 0.0178	**0.0004**	**0.001206**	**0.0187**	0.4735
	450	0.8134 + 0.0135	0.8240 + 0.0071	0.8304 + 0.0147	0.6778	-	-	-
	550	0.8234 + 0.0126	0.8236 + 0.0066	0.8257 + 0.0137	0.9892	-	-	-
LEC 2	390	0.1052 + 0.0171	0.0166 + 0.0090	0.0422 + 0.0186	**0.0001**	**5.96E-06**	**0.0156**	0.3230
	450	0.0491 + 0.0144	0.0119 + 0.0076	0.0102 + 0.0157	0.0675	-	-	-
	550	0.0186 + 0.0136	-0.0198 + 0.0071	-0.0057 + 0.0147	**0.0442**	0.4995	0.3317	0.3216

The histological grouping is most evident at 390nm, where the intensity, lifetime, LEC 1 and LEC 2 show statistical differences with at least one grouping via ANOVA p-values (in bold). At the 450nm band, only the intensity parameter yielded significantly significant results. At 550nm, both the lifetime parameter and LEC 2 was statistically significant. This trend of lower wavelengths yielding more statistically meaningful results matches previous findings: thin plaques generally show the most dramatic changes in intensity between thin and thick plaques at 390 nm. In addition, lifetimes for elastin-rich regions were shorter than collagen-rich regions at 390nm (38). It is important to note that these trends are observed with plaque samples containing very little lipids. The p-values reported on Table 2 also show that the fibrocalcified plaque is indistinguishable from fibrotic plaque. Fibrocalcified plaques were generally thick layers of plaque over 100μm. Because calcium does not possess a strong fluorescent signal, collagen dominated the fluorescence emission of these samples. Figure 4 shows a multicomparison of the statistically significant parameters outlined in bold in Table 2.

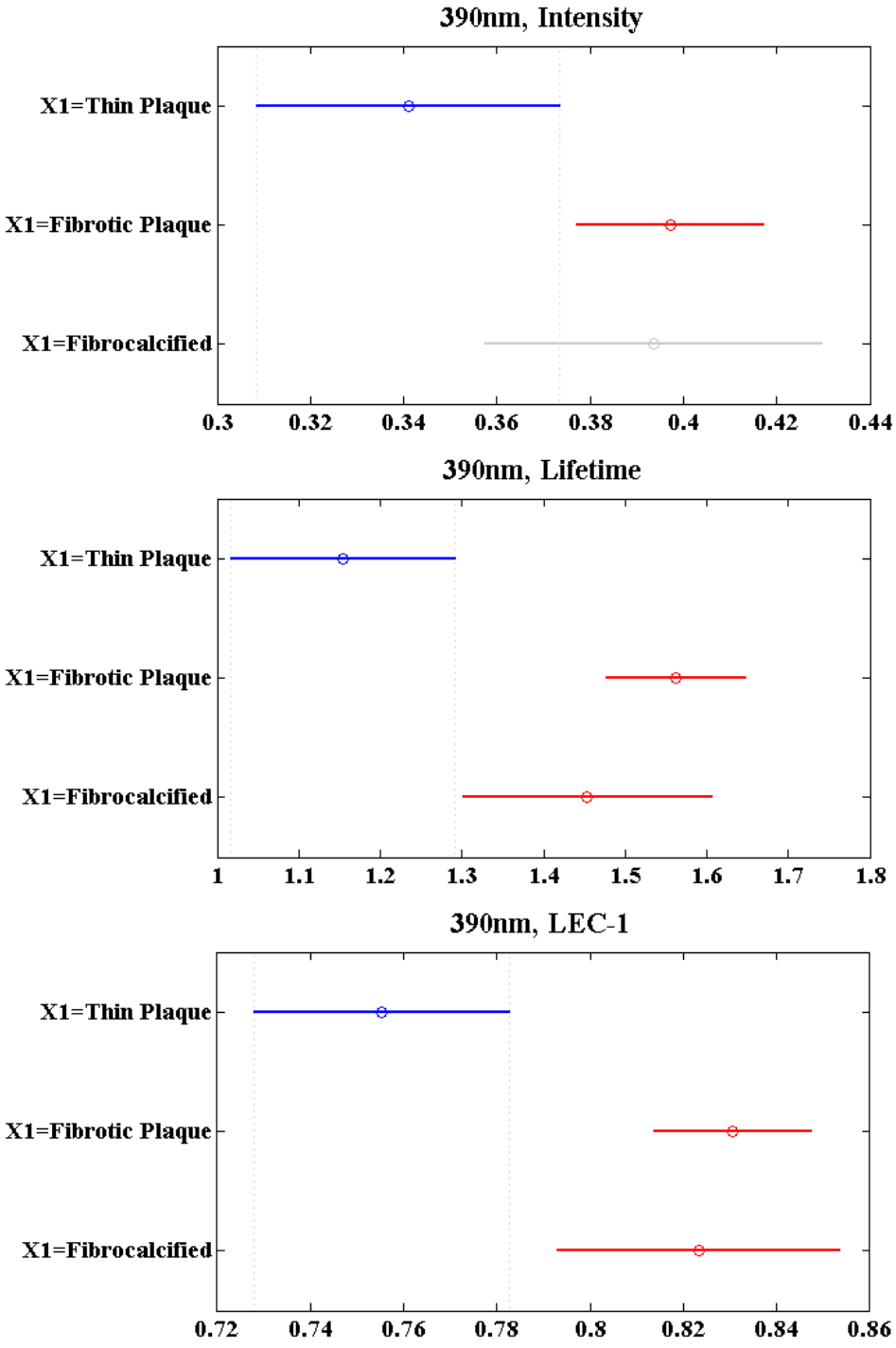

Figure 4. Multicomparison test results of significant ($p<0.05$) parameters when analyzing by histological grouping. 100µm threshold between thin and fibrotic plaques.

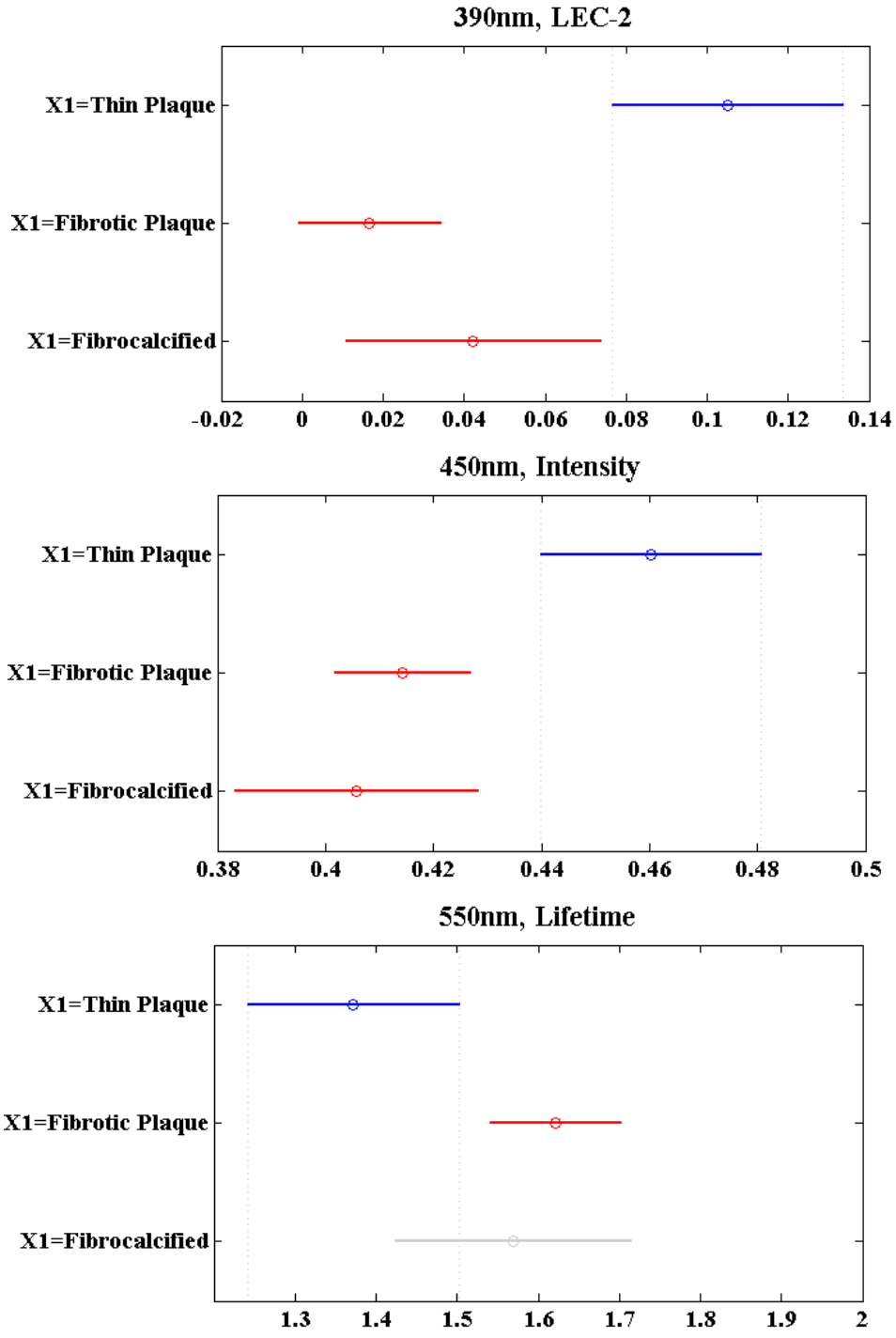

Figure 4. Continued.

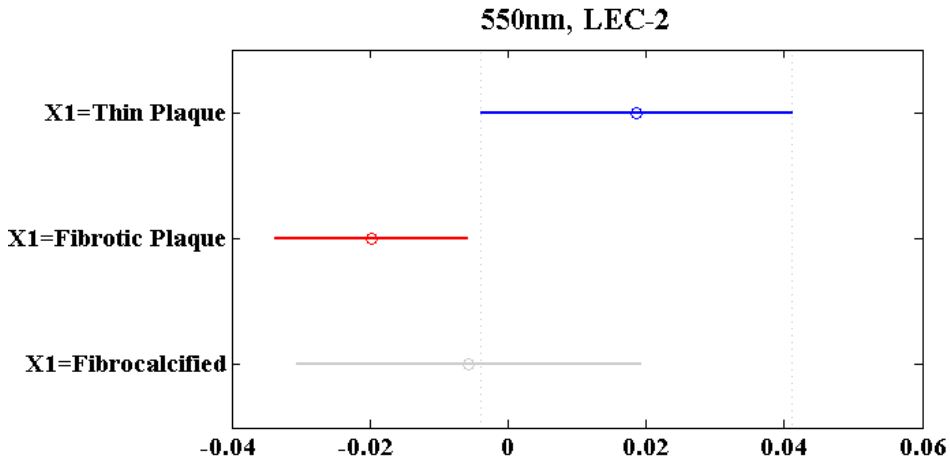

Figure 4. Continued

4.3.2 Fibrotic Plaque Thickness Analysis

An analysis of fibrotic plaque thickness was also performed. Thin and fibrotic and plaques were grouped into categories by thickness range, and their average intensity and lifetime were compared at 390 nm and 450 nm wavelengths. The results are displayed on Figure 5.

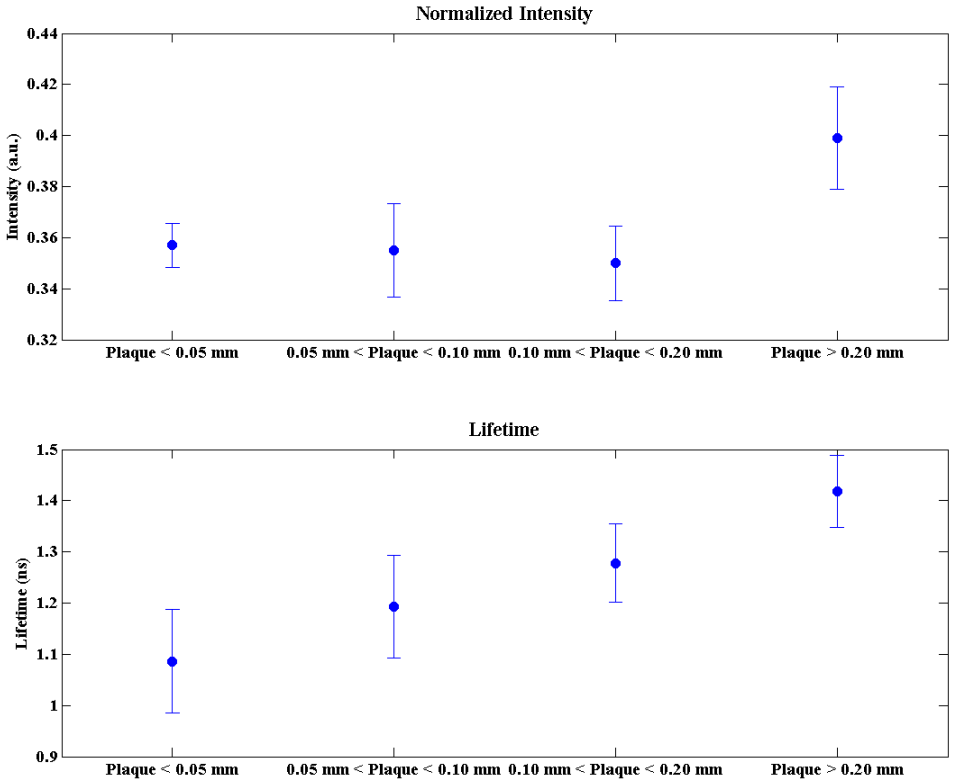

Figure 5. Intensity (top) and lifetime (bottom) Comparison of data grouped by plaque thickness at 390 nm. Error bars denote standard error.

The intensity (top) data on figure 5 shows that the values remain fairly constant as thickness increases, but there is a sudden shift in intensity for both wavelengths when the plaques grow beyond 0.20 mm thickness. Beyond this, the intensity at both wavelengths converge and broaden in their intensity reading (hence the large standard deviation).

The lifetime (bottom) values show a more gradual shift as thickness increases. At 0.10 mm, the wavelength measurements merge. The overall positive trend between

plaque thickness and lifetime at 390nm is expected, and corresponds with previous work (38).

5. DISCUSSION AND CONCLUSIONS

5.1 Discussion

This study tests the validity of our Fluorescence Lifetime Imaging Microscopy (FLIM) system to differentiate atherosclerotic plaque types into several histological groupings: Thin, fibrotic, thin cap FA, thick cap FA, and fibrocalcified plaques. After recording temporally resolved images of the artery samples at three critical wavelengths (390nm, 450nm, and 550nm) (38), we performed Laguerre deconvolution on the samples to obtain the true fluorescent response, which has been reported to be advantageous over least-square iterative reconvolution (39). Using histological sample classifications to categorize the FLIM images into these groups, statistical analyses were performed in order to determine if the relative intensity, lifetime measurement, and Laguerre expansion coefficients may be used to differentiate histological groupings. The findings of this study are in agreement with previous results in that thin plaque is differentiable from fibrotic plaque and thick cap FA plaques. There were not enough thin cap FA plaques in the dataset, however, to draw any statistically significant conclusions regarding the system's ability to successfully detect shallow lipid cores. The following section discusses the results of the study, their implications, and problems that should be addressed.

In order to decrease computation requirements, the α parameter used in Laguerre deconvolution was investigated in an attempt to set it to a single value. The α optimization, discussed in section 3.4.2, determined an optimal value for calculating the

Lageurre expansion coefficients in all samples. The α value was determined to be α=0.8118. Doing so proved to be much less computationally expensive than optimizing on a sample-by-sample model and allowed the expansion coefficients and lifetimes to be determined and compared to all samples in the experimental data set. There were limitations in doing this, however. By setting a static value that is not optimized by a case by case basis, the Laguerre fits are not perfect, and may adversely affect lifetime calculations. However, all fits had less than 5% error between the estimated response curves constructed by LEC coefficients and recorded response curve.

The results from ANOVA testing of cap thickness (section 4.4.1) did not yield a difference between fibrotic plaque and thick-cap FA. This is expected, because a large collagen region thicker than the penetration depth of the excitation beam will return primarily a collagen signature. A 100μm threshold was used to differentiate thin plaques and thick fibrotic plaque classifications. This threshold was able to differentiate thin plaque, whose fluorescent signal is dominated by elastin, from thick plaque, whose fluorescent signal is dominated by collagen. Fibrocalcified plaques displayed an emission very similar to fibrotic plaques. Calcification is a sign of a late-stage plaque, and can be detected by some other intravascular modalities, namely IVUS and Electron beam computed tomography (EBCT) (40). The fibrocalcified samples were generally thick. Because collagen is the primary fluorophore in normal plaque without lipids, it made up the majority of the signal for plaques labeled as fibrocalcified. For many of the statistically significant parameters (Lifetime, LEC-1, LEC-2 at 390nm, and Intensity at 450nm), fibrocalcified plaque was discernable from thin plaques. Additionally, there

were no thin-cap FA samples. A larger dataset may have yielded vulnerable plaques in order to analyze. Analysis by cholesterol composition was similar to analysis by plaque thickness and calcification. Cholesterol-laden plaque, which was plaque containing cholesterol and foam cells within the first 200μm of the lesion, followed the same trend as fibrotic plaque and was statistically different only from thin plaque, indicating that collagen dominated the FLIM signal.

When investigating FLIM signals as a function of plaque thickness, both intensity and lifetime measurements at 390 nm correlated to sample's dominant fluorophores. The change in intensity was very sudden as plaque thickness grew above 0.20 mm, however. In contrast, lifetime measurements of plaque showed a more gradual trend of increasing lifetime with plaque thickness, beginning at ~1.1 ns for plaques less than 0.05 mm thick, rising to 1.55 ns with plaques greater than 0.20 mm thick. This gradual shift suggests that lifetime may indirectly reflect plaque thickness. To determine if this is a meaningful trend, this test should be performed on a larger dataset. This analysis should also be performed with thin-plaque samples at 390 nm and 550 nm: 390 nm to discern cap thickness, and 550 nm to determine lipid content of the underlying core.

Both analyses provided consistent trends that matched previous studies (38). However, some inconsistencies exist with previous research, namely lifetime measurements of fibrotic plaque, whose primary fluorophore is collagen. This study found that collagen-dominated plaques had an average lifetime of 1.56ns, 1.49ns, and 1.62ns for 390nm, 450nm, and 550nm wavelengths, respectively (See: Table 2). Thick

plaque lifetime values in previous studies yielded higher lifetime values at 2 ns for 390 nm, however (38). Elastin-dominated plaque lifetimes were within acceptable range, and also generally lower than collagenous plaques with lifetimes of 1.15ns, 1.41ns, and 1.37ns for 390nm, 450nm, and 550nm, respectively. This indicates a possible discrepancy in calculating the lifetime. Although the fits between the estimated Laguerre response and the measured response had very small errors (<5% in all cases), lifetime values were not as high as expected. A closer look into the α parameter optimization may be necessary to explore the reasoning behind this, however. The set α value used in this study was determined by a previous dataset, and may not have fully represented the dataset collected for statistical analysis.

The single-lifetime modeling scheme used in this study calculates a single lifetime value, and has the advantage of being computationally less expensive than multi-lifetime models, such as multiexponential approximations, due to its deconvolution technique (35). However, the downside to this is that a multi-fluorophore sample, such as arterial plaques, will not have all fluorophores directly represented by the model. This problem is rectified by the model used to represent the decay curve: Lageurre deconvolution is a summation of decaying lageurre curves, and is a function of both lageurre expansion coefficients and the α parameter, both optimized to estimate the time-resolved fluorescence emissions. Because this model uses multiple expansion coeffiencents to estimate the emission curve, it is safe to say that the Lageurre coefficients may be able to differentiate multiple fluorophores inside a sample. It is important to recognize that these expansion coefficients function similarly to a

summation of decay curves with multiple time-constants in that they make up the total decay. However, it would be advantageous to perform a comparison between the lageurre coeffiecients and multiexponential lifetime coefficients for different plaque types. Doing so will allow for a more sound comparison between studies that utilize the multiexponential lifetime model. Using a multiexponential model also takes into account the multiple fluorophores found in the field of view.

5.2 Future Scope

Testing on the current FLIM system should be expanded to fully analyze the ability of this FLIM angioscopy prototype to detect vulnerable plaques. As discussed above, several problems exist that should be addressed, such as unusually low lifetimes of collagen and the lack of vulnerable plaque samples. A future study should further investigate lifetime as a function of plaque thickness and determine why the lifetime values in this study are lower than normal in the case of fibrotic plaques. If the trend between lifetime and plaque thickness holds true for future tests, thin-cap FA samples should be measured at both 390 nm and 550 nm wavelengths. By using 550 nm to confirm or deny lipid core presence, lifetime at 390 nm may reflect cap thickness rather than plaque thickness. Future studies should also focus on the edge of plaque lesions in order to increase the chance to image vulnerable regions. Additionally, future studies should seek to image vessel samples that are not laid flat, with their shape intact. This should provide a more realistic view of the vessels imaged. Finally, a study of compiled thin-cap FA plaques must be performed against both thin plaques and fibrotic plaques.

Another course would be to utilize the strengths of FLIM as a biochemical detection scheme to supplement other optical angioscopy techniques, namely OCT. Its potential has been established recently (29), and may produce positive results in identifying vulnerable plaque, among other histological conditions.

5.3 Conclusions

A FLIM angioscopy system and post-processing techniques have been tested for their ability to analyze coronary artery samples for their biochemical content. The Laguerre deconvolution method used to process the data has proved to be efficient at extracting the impulse response in excised coronary vessel lumen. Several experiments have been proposed to further validation testing of the current FLIM system, including correlating plaque thickness to lifetime measurements and an extended, focused study on thin-cap FA specimens. The trends presented here show potential for the current FLIM and statistical analysis system to identify plaques; provided several processing techniques are made to correct for errors that have been identified and discussed in this research summary.

REFERENCES

1. Marcu, L., M. Fishbein, J. Maarek, and W. Grundfest (2001) Discrimination of human coronary artery atherosclerotic lipid-rich lesions by time-resolved laser-induced fluorescence spectroscopy. *Arteriosclerotisis, Thrombosis, and Vascular Biology.* **21,** 1244-1250.
2. Marcu, L., Q. Fang, J. Jo, T. Papaioannou, and A. Dorafshar, et al. (2005) In vivo detection of macrophages in a rabbit atherosclerotic model by time-resolved laser-induced fluorescence spectroscopy. *Atherosclerosis.* **181,** 295-303.
3. Pfefer, T., D. Paithankar, J. Ponero, K. Schomacker, and N. Nishioka (2003) Temporally and spectrally resolved fluorescence spectroscopy for the detection of high grade dysplasia in Barrett's esophagus. *Lasers in Surgery and Medicine.* **32,** 10-16.
4. Inoue, T., N. Uedo, R. Ishihara, T. Kawaguchi, and N. Kawada, et al. (2010) Autofluorescence imaging videoendoscopy in the diagnosis of chronic atrophic fundal gastritis. *Journal of Gastroenterology.* **45,** 45-51.
5. Eichhorn, R., G. Wessler, M. Scholz, D. Leupold, and G. Stankovic, et al. (2009) Early diagnosis of melanotic melanoma based on laser-induced melanin fluorescence. *Journal of Biomedical Optics.* **14,** 034033.
6. Rosamond, W., K. Flegal, K. Furie, A. Go, and K. Greenlund, et al. (2007) Heart disease and stroke statistics- 2008 update: a report from the american heart association statistics committee and stroke statistics subcommittee. *Circulation.* **117,** 1-123.
7. Virmani, R., R. Kolodgie, A. Burke, A. Farb, and S. Schwartz (2000) Lessons from sudden coronary death: a comprehensive morphological classification scheme for atherosclerotic lesions. *Aterioscleroses, Thrombosis, and Vascular Biology.* **20,** 1262-1275.
8. Virmani, R., R. Kolodgie, A. Burke, and A. Farb (2002) Vulnerable plaque: the pathology of unstable coronary lesions. *Journal of Intervention Cardiology and Electrophysiology.* **15,** 439 - 446.
9. Tearney, G., I. Jang, and B. Bouma (2006) Optical coherence tomography for imaging the vulnerable plaque. *Journal of Biomedical Optics.* **11,** 021002.
10. Kume, T., T. Akasaka, T. Kawamoto, N. Watanabe, and E. Toyota, et al. (2006) Assessment of coronary arterial plaque by optical coherence tomography. *The American Journal of Cardiology.* **97,** 1172-1175.
11. Kaple, R., A. Maehara, K. Sano, E. Missel, and C. Castellanos, et al. (2009) The axial distribution of lesion-site atherosclerotic plaque components: An in vivo volumetric intravascular ultrasound radio-frequency analysis of lumen stenosis, necrotic core and vessel remodeling. *Ultrasound in Med. & Biol.* **35,** 550-557.
12. MacNeill, B., I. Jang, B. Bouma, N. Iftimia, and M. Takano, et al. (2004) Focal and multi-focal plaque macrophage distributions in patients with acute and stable presentation of coronary artery disease. *Journal of the American College of Cardiology.* **44,** 972-979.

13. MacNeill, B., B. Bouma, H. Yabushita, I. Jang, and G. Tearney (2005) Intravascular optical coherence tomography: cellular imaging. *Journal of Nuclear Cardiology.* **12,** 460-465.
14. Nadkarni, S., B. Bouma, J. de Boer, and G. Tearney (2009) Evaluation of collagen in atherosclerotic plaques: the use of two coherent laser-based imaging methods. *Lasers Med Science.* **24,** 439-445.
15. Zysk, A., F. Nguyen, A. Oldenburg, D. Marks, and S. Boppart (2007) Optical coherence tomography: a review of clinical development from bench to bedside. *Journal of Biomedical Optics.* **12,** 051403.
16. Anastassopoulou, N., B. Arapoglou, and P. Demakakos (2001) Spectroscopic characterization of carotid atherosclerotic plaque by laser induced fluorescence. *Laser Surgery Medicine.* **28,** 67-73.
17. Marcu, L., J. Jo, Q. Fang, T. Papaionnou, and T. Reil, et al. (2009) Detection of rupture-prone atherosclerotic plaques by time-resolved laser-induced fluorescence spectroscopy. *Atherosclerosis.* **204,** 156-164.
18. Rocha, R., A. Villaverde, L. Silveira Jr., M. Costa, and L. Alves, et al. (2008) Identification of atherosclerotic plaques in carotid artery by fluorescence spectroscopy. *AIP Conference Proceedings.* **992,** 1151-1155.
19. Moreno, P. and J. Muller (2003) Detection of high-risk atherosclerotic coronary plaques by intravascular spectroscopy. *Journal of Interventional Cardiology.* **16,** 243-252.
20. Scepanovic, O., M. Fitzmaurice, J. Gardecki, G. Anghuloiu, and S. Awasthi, et al. (2006) Detection of morphological markers of vulnerable atherosclerotic plaque using multimodal spectroscopy. *Journal of Biomedical Optics.* **11,** 021007.
21. Rocha, R., L. Silveira Jr., A. Villaverde, C. Pasqualucci, and M. Costa, et al. (2007) Use of near-infrared raman spectroscopy for identification of atherosclerotic plaques in the carotid artery. *Photomedicine and Laser Surgery.* **25,** 482-486.
22. Caplan, J., S. Waxman, R. Nesto and J. Muller (2006) Near-Infrared Spectroscopy for the Detection of Vulnerable Coronary Artery Plaques. *Journal of American College of Cardiology.* **47,** C92-C96.
23. Hamdan, A., A. Assali, S. Fuchs, A. Battler and R. Komowski (2007) Imaging of Vulnerable Coronary Artery Plaques. *Catheterization and Cardiovascular Interventions.* **70,** 65-74.
24. Lilledahl, M., O. Haugen, L. Randeberg, and L. Svaasand (2005) Characterization of atherosclerotic plaque by reflection spectroscopy and thermography: a comparison. *Proc. of SPIE.* **5686,** 415-425.
25. Lakowicz, J. (2006) *Principles of Fluorescence Spectroscopy.* Springer, New York, NY.
26. Laughlin, S. (2008) In vivo imaging of membrane-associated glycans in developing zebrafish. *Science.* **320,** 664-667.
27. Lempert, W. and S. Harris (2000) Flow tagging velocimetry using caged dye photo-activated fluorophores. *Measurement Science & Technology.* **11,** 1251-1258.

28. The IceCube Research Group (2010) Fluorescence. Available at: http://icecube.berkeley.edu/~bramall/work/astrobiology/fluorescence.htm. Accessed on 14 March 2010.
29. Applegate, B., J. Jo, and F. Clubb (2009) Morphological and biochemical imaging of coronary atherosclerotic plaques using optical coherence tomography and fluorescence lifetime imaging. *Cardiovascular Research Technologies.* **10,** 210-211.
30. Gregoire, J., W. Edwards, M. Jeong, A. Camrud, and A. Lerman, et al. (1997) Short wave ultraviolet laser energy in porcine coronary arteries: Medical cell death and neointimal formation. *Lasers in Surgery and Medicine.* **21,** 374-83.
31. Maarek, J., L. Marcu, W. Snyder, and W. Grundfest (2000) Time-resolved fluorescence spectra of arterial fluorescent compounds: Reconstruction with the laguerre expansion technique. *Photochemistry and Photobiology.* **71,** 178-187.
32. Johnson, M. and S. Frasier (1985) Non-linear least-square analysis. *Methods Enzymology*. **117**.
33. Ware, W., L. Doemeny, and T. Nemzek (1973) Deconvolution of fluorescence and phosphorescence decay curves. A least square method. *J. Phys. Chem.* **77,** 2038–2048.
34. Periasamy, A., K. Sharman, and J. Demas (1999) Fluorescence lifetime imaging microscopy using rapid lifetime determination method: Theory and applications. *Biophysics Journal.* **76,** A10.
35. Jo, J., Q. Fang, and L. Marcu (2005) Ultrafast method for analysis of fluorescence lifetime imaging microscopy data based on the laguerre expansion technique. *IEEE Journal.* **11,** 835-845.
36. Ramanujan, V., J. Jo, G. Cantu, and B. Herman (2008) Spatially resolved fluorescence lifetime mapping of enzyme kinetics in living cells. *Journal of Microscopy.* **230,** 329-338.
37. Dabir, A., C. Trivedi, Y. Ryu, P. Pande, and J. Jo (2009) Fully automated deconvolution method for on-line analysis of time-resolved fluorescence sectroscopy data based on an iterative Laguerre expansion technique. *Journal of Biomedical Optics.* **14,** 024030.
38. Thomas, P., P. Pande, F. Clubb, J. Adame, and J. Jo (2010) Biochemical imaging of human atherosclerotic plaques with fluorescence lifetime angioscopy. *Photochemistry and Photobiology.* **86,** 727-731.
39. Dabir, A. (2009) Automation of the Laguerre Expansion Technique for Analysis of Time-Resolved Fluorescence Spectroscopy Data. Master's thesis, Texas A&M University, College Station.
40. Cham, B. (2001) Plaque cholesterol and calcium: the value of EBCT in the detection of coronary atherosclerosis. *European Journal of Clinical Investigation.* **31,** 471-475.

APPENDIX

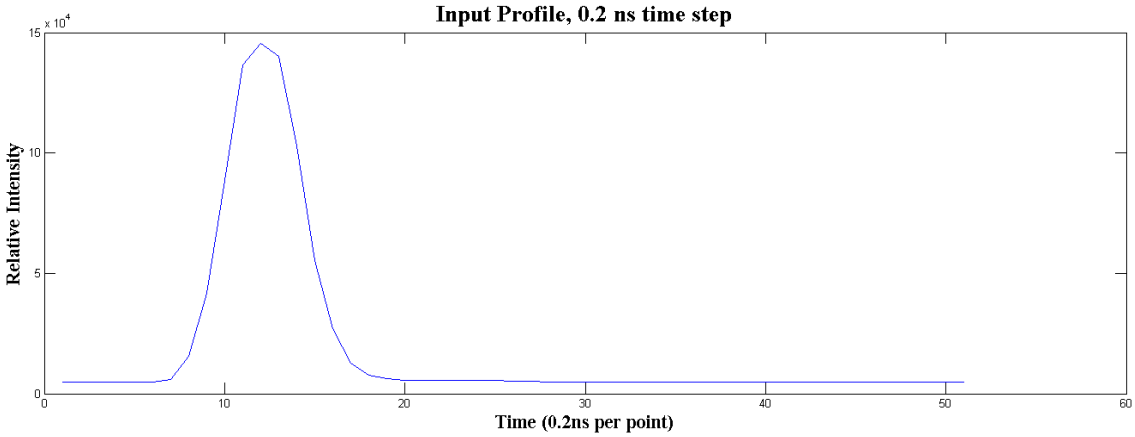

Figure A-1. Recorded instrument response x(n) used to deconvolve samples.

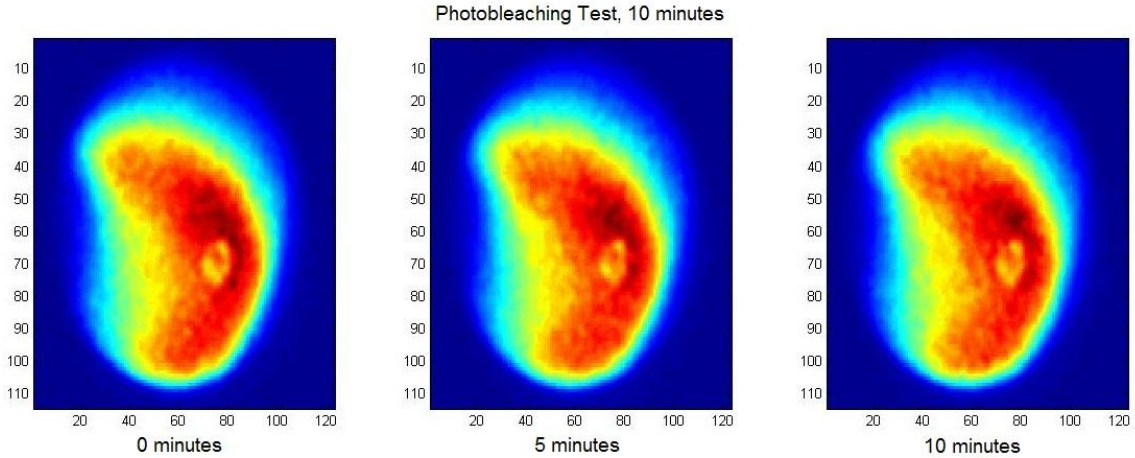

Figure A-2. Photobleaching effect on coronary tissue sample over 10 minutes.

VITA

Name:	Patrick Allen Thomas
Address:	Department of Biomedical Engineering c/o Dr. Javier Jo Texas A&M University College Station, TX 77843-3121
Email Address:	pthomas0786@gmail.com
Education:	B.S., Biomedical Engineering, Louisiana Tech University, 2008 M.S., Biomedical Engineering, Texas A&M University, 2010